



# Cavity Pattern Formation and Its Dynamics of Fiber Fuse in Single-Mode Optical Fibers

Yoshito Shuto 

Ofra Project, Iruma City, Japan

ofra@tuba.ocn.ne.jp

**Received:** August 31, 2020

**Accepted:** October 26, 2020

**Published:** December 31, 2020

**Abstract.** The nonlinear oscillation model using the Van der Pol equation was able to phenomenologically explain the formation of periodic cavities, the cavity shape, and the regularity of the cavity pattern in the core layer as a result of the relaxation oscillation and cavity compression and/or deformation. We assumed the relationships between the parameters of the population dynamics of interacting self-oscillators using the Kuramoto model and the fiber fuse propagation, and found an equation describing the power dependence of the periodic cavity interval. The experimentally determined cavity intervals at  $P_{th} \leq P_0 \leq 5$  W satisfied this equation. Furthermore, the experimental cavity intervals at  $P_0 > 6$  W can be explained by considering the power dependence of the propagation velocity of the fiber fuse and the constant period of the Van der Pol oscillator.

**Keywords.** Nonlinear oscillation model; Van der Pol equation; Fiber fuse phenomenon; Kuramoto model

**MSC.** 34C15 Nonlinear oscillations; Coupled oscillators

Copyright © 2020 Yoshito Shuto. This is an open access article distributed under the Creative Commons Attribution License, which permits unrestricted use, distribution, and reproduction in any medium, provided the original work is properly cited.

## 1. Introduction

The fiber fuse phenomenon was first observed in 1987 by British scientists [24], [25], [28], [29]. A fiber fuse can be generated by bringing the end of a fiber into contact with an absorbent material or melting a small region of a fiber using an arc discharge of a fusion splice machine [28], [30], [46], [47]. If a fiber fuse is generated, an intense blue-white flash occurs in the fiber core, and this flash propagates along the core in the direction of the optical power source.

The core layer in which the fuse propagates is seriously damaged, and the damage has the form of periodic bullet-shaped cavities (or occasionally nonperiodic filaments) remaining in the core [3], [4], [6], [12–16], [18–21], [24], [25], [28–30], [34], [35], [46–51], as shown in Figure 1.

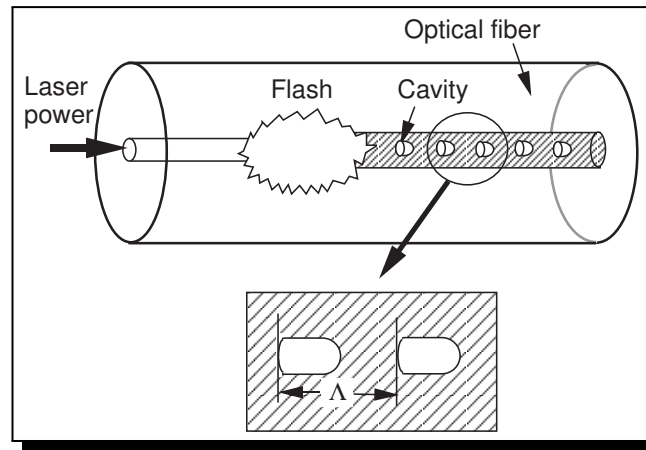


Figure 1. Schematic view of damaged optical fiber.

In this figure  $\Lambda$  is the periodic cavity interval. The cavity patterns owing to the fiber fuse in single-mode fibers can be classified into the three patterns shown in Figure 2, where  $l$  is the length of the cavity.

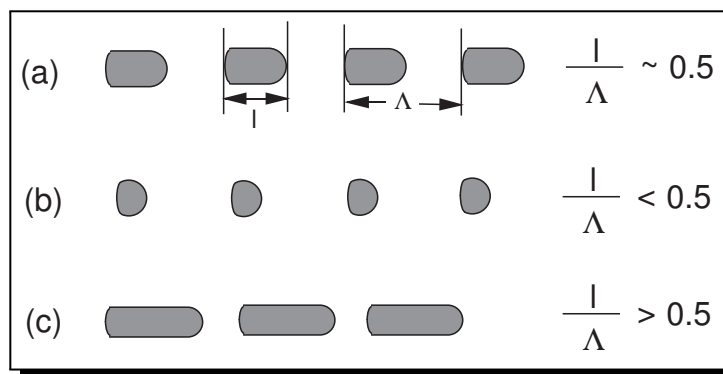


Figure 2. Cavity patterns observed in optical fiber.

The observed periodic cavity patterns belong to patterns (a)-(c) with the pattern depending on the value of  $l/\Lambda$ .

The detection systems for fiber fuse have been proposed by several research institutes, which use FBG sensors [36], an optical time-domain reflectometer [1], and an optical frequency-domain reflectometer [27]. Recently, several types of optical fiber sensors based on periodic cavities have been proposed as a cost-effective approach to sensor production [3], [18–21]. For sensor applications, the precise control of  $l$  and/or  $\Lambda$  is very important.

These cavities have been considered to be the result of either the classic Rayleigh instability caused by the capillary effect in the molten silica surrounding a vaporized fiber core [4] or the electrostatic repulsion between negatively charged layers induced at the plasma-molten

silica interface [58–60]. However, these models cannot explain in depth to form several cavity patterns shown in Figure 2 and the precise values of  $l$  and/or  $\Lambda$  cannot be estimated by using these models.

Recently, the author has proposed a novel nonlinear oscillation model, where the oscillatory motion of the ionized gas plasma during fiber fuse propagation behaves as a Van der Pol oscillator, and qualitatively explained both the silica-glass densification and cavity pattern formation observed in fiber fuse propagation by using this model [41], [42]. In this paper, the author at first describes the nonlinear oscillation model using the Van der Pol equation and cavity pattern formation observed in fiber fuse propagation.

The Van der Pol oscillator is a classical model for self-oscillating relaxation systems which, after initial amplitude growth, reach a limit cycle in phase space due to a nonlinear saturation mechanism. The reason for the occurrence of the rhythmical interaction of many Van der Pol oscillators in the fiber fuse initiation process, at which the cavities are formed, has not been studied in detail theoretically. Therefore, in the latter part of this paper, the author describes the initiation process of the fiber fuse on the basis of the population dynamics of interacting self-oscillators.

## 2. Nonlinear Oscillation Behavior in Ionized Gas Plasma

A low-frequency plasma instability is triggered by moving the high-temperature front of a fiber fuse toward the light source. It is well known that such a low-frequency plasma instability behaves as a Van der Pol oscillator with the natural frequency  $\omega_0$  (see literatures listed in [41]).

The density  $\rho$  of the plasma is assumed to be in the form  $\rho = \rho_0 + \rho_1$ , where  $\rho_0$  is the initial density of the stationary (unperturbed) part in the front region of the plasma and  $\rho_1$  is the perturbed density. In the following calculation, we divided  $\rho_1$  by  $\rho_0$  and used this value as  $\rho_1$ .

The dynamical behavior of  $\rho_1$  resulting from fiber fuse propagation can be represented by the Van der Pol equation

$$\frac{d^2\rho_1}{dt^2} - \epsilon(1 - \beta\rho_1^2 + 2\zeta\rho_1)\frac{d\rho_1}{dt} + \omega_0^2\rho_1 = 0, \quad (2.1)$$

where  $\epsilon$  is a parameter that characterizes the degree of nonlinearity and  $\beta$  characterizes the nonlinear saturation (see [41, Appendix B]). The nonlinearity parameter  $\zeta$  characterizes the oscillation pattern.

The natural frequency  $\omega_0$  of the oscillation of the gas plasma is determined by the ion-sound velocity  $C_s$  and the free-running distance  $L_f$  of the ion-sound wave, and is given by

$$\omega_0 = 2\pi f = 2\pi \frac{C_s}{L_f}, \quad (2.2)$$

where  $f$  is the frequency of the oscillation of the gas plasma, which is estimated to be about 1 MHz [42].

The oscillatory motion for  $\epsilon = 7.5$ ,  $\beta = 6.5$ , and  $\zeta = 0$  was calculated using Eq. (2.1). The calculated result is shown in Figure 3, where the perturbed density  $\rho_1$  is plotted as a function of time.

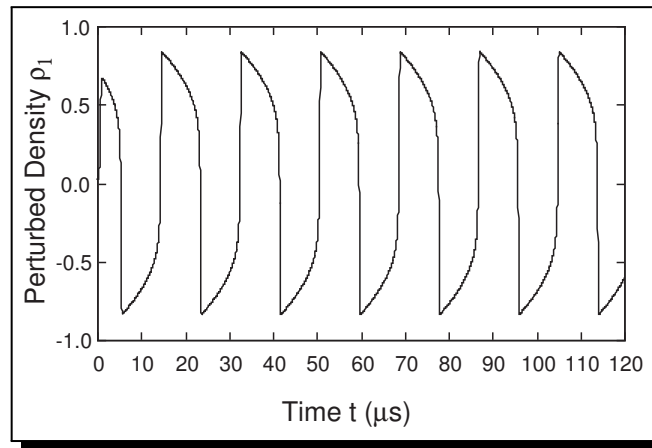


**Figure 3.** Time dependence of the perturbed density during fiber fuse propagation.  $\epsilon = 7.5, \beta = 6.5, \zeta = 0$ .

It can be seen that for  $\epsilon = 7.5$ , the oscillations consist of sudden transitions between compressed and rarefied regions. This type of motion is called a relaxation oscillation [55]. The period  $\Phi$  of the motion corresponding to  $\epsilon = 7.5$  was estimated to be about  $18.08 \mu\text{s}$ .

The oscillatory motion generated in the high-temperature front of the ionized gas plasma can be transmitted to the neighboring plasma at the rate of  $V_f$  when the fiber fuse propagates toward the light source. Figure 4 shows a schematic view of the dimensional relationship between the temperature and the perturbed density of the ionized gas plasma during fiber fuse propagation.

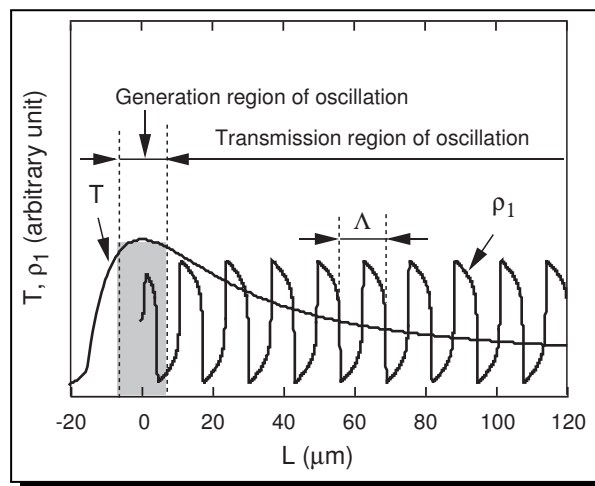


**Figure 4.** Schematic view of the dimensional relationship between the temperature and the perturbed density of the ionized gas plasma during fiber fuse propagation.

In Figure 4,  $\Lambda$  is the interval between the periodic compressed (or rarefied) parts.

The relationship between the period  $\Phi$  and the interval  $\Lambda$  is

$$\Lambda = \Phi V_f, \tag{2.3}$$

where  $V_f$  ( $\sim 1 \text{ m/s}$ ) is the propagation velocity of the fiber fuse. The  $\Lambda$  value of the motion corresponding to  $\epsilon = 7.5$  is estimated to be about  $18.08 \mu\text{m}$  using Eq. (2.3) and  $V_f = 1 \text{ m/s}$ .

If a large amount of molecular oxygen ( $O_2$ ) accumulates in the rarefied part, the periodic formation of bubbles (or cavities) will be observed. In such a case,  $\Lambda$  is equal to the periodic cavity interval. The estimated  $\Lambda$  value ( $18.08 \mu\text{m}$ ) is close to the experimental periodic cavity intervals of  $13\text{--}22 \mu\text{m}$  observed in fiber fuse propagation [48], [52].

Figure 5 shows the relationship between  $\Phi$  and the nonlinearity parameter  $\epsilon$ .

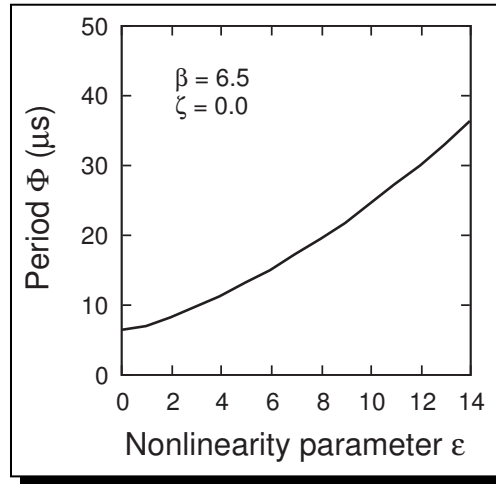


**Figure 5.** Relationship between the period  $\Phi$  and the nonlinearity parameter  $\epsilon$ .  $\beta = 6.5$ ,  $\zeta = 0$ .

As shown in Figure 5,  $\Phi$ , which is proportional to the interval  $\Lambda$ , increases with increasing  $\epsilon$ . That is, the increase in  $\Phi$  and/or  $\Lambda$  occurs because of the enhanced nonlinearity. It was found that the experimental periodic cavity interval increases with the laser pump power [48], [52]. It can therefore be presumed that the nonlinearity of the Van der Pol oscillator occurring in the ionized gas plasma is enhanced with increasing pump power.

Kashyap reported that the cavity shape was dependent on the nature of the input laser light (CW or pulses) [29], [30]. Todoroki classified the damage to the front part of a fiber fuse into three shapes (two spheroids and a long partially cylindrical cavity) depending on the pump power [48]. He also found that a rapid increase or decrease in the pump power results in an increase in the length of the cavity-free segment or the occurrence of an irregular cavity pattern, respectively [51]. These findings indicate that the cavity shape and the regularity of the cavity pattern may be determined by the degree of nonlinearity of the Van der Pol oscillator.

### 3. Effect of Nonlinearity Parameters on Cavity Patterns

The nonlinearity parameter  $\zeta$  characterizes the oscillation pattern. The oscillatory motion for  $\epsilon = 7.5$ ,  $\beta = 6.5$ , and  $\zeta = 0$  was shown in Figure 3, where the perturbed density  $\rho_1$  is plotted as a function of time. It can be seen in Figure 3 that the oscillations consist of sudden transitions between compressed and rarefied regions, and the retention time  $\tau_r$  of the rarefied regions equals that of the compressed regions  $\tau_c$ . The relationship between the period  $\Phi$  ( $= \tau_r + \tau_c$ ) and the interval  $\Lambda$  is given by Eq. (2.3), and the relationship between  $\tau_r$  and the length  $l$  of the cavity is

$$l = \tau_r V_f. \quad (3.1)$$

The  $\Lambda$  and  $l$  values of the motion corresponding to  $\epsilon = 7.5$ ,  $\beta = 6.5$ , and  $\zeta = 0$  are estimated to be about 9.04 and 18.08  $\mu\text{m}$ , respectively, using Eqs. (2.3) and (3.1) and  $V_f = 1$  m/s. That is,  $l/\Lambda = 0.5$  in the case of  $\zeta = 0$ .

Next, the oscillatory motion for  $\zeta = 2$  and  $-2$  with  $\epsilon = 7.5$  and  $\beta = 6.5$  was examined. The calculated results are shown in Figures 6 and 7, respectively.

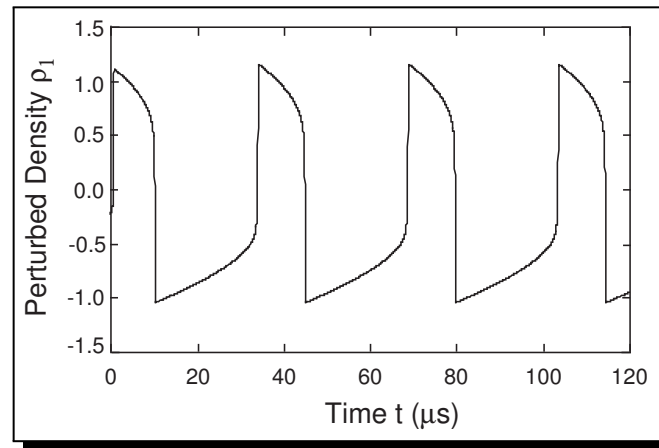


**Figure 6.** Time dependence of the perturbed density during fiber fuse propagation.  $\epsilon = 7.5$ ,  $\beta = 6.5$ ,  $\zeta = 2$ .

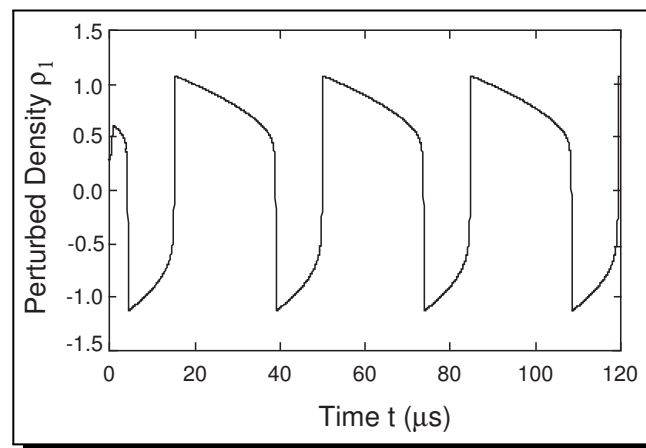


**Figure 7.** Time dependence of the perturbed density during fiber fuse propagation.  $\epsilon = 7.5$ ,  $\beta = 6.5$ ,  $\zeta = -2$ .

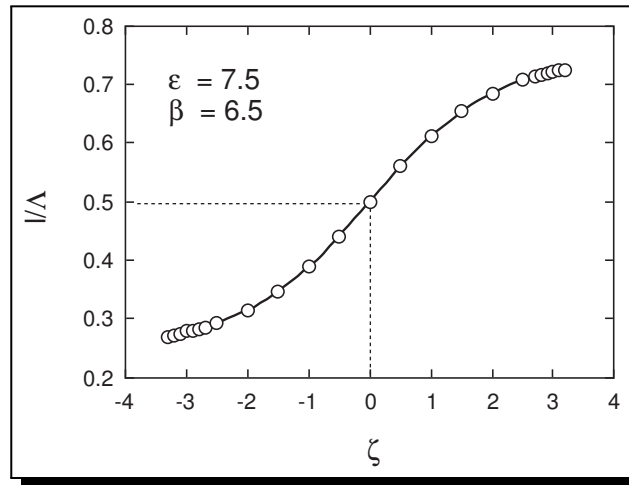
As shown in Figure 6, the retention time  $\tau_r$  of the rarefied regions is larger than that of the compressed regions  $\tau_c$ . As a result, the ratio  $l/\Lambda$  is larger than 0.5 in the case of  $\zeta = 2$ . On the other hand, as shown in Figure 7,  $\tau_r$  is smaller than  $\tau_c$  and  $l/\Lambda < 0.5$  in the case of  $\zeta = -2$ .

Figure 8 shows the relationship between  $l/\Lambda$  and the nonlinearity parameter  $\zeta$ .

As shown in Figure 8,  $l/\Lambda$  increases with increasing  $\zeta$  and approaches its maximum value (about 0.724) at  $\zeta \sim 3.1$ . In contrast,  $l/\Lambda$  approaches its minimum value (about 0.268) at  $\zeta \sim -3.3$ .

The large  $l/\Lambda$  ( $> 0.5$ ) of the cavity was observed in the fiber fuse initiation process [46], [47] and a varicose instability in the damaged fiber [4]. In contrast, small  $l/\Lambda$  ( $< 0.5$ ) was observed in the self-termination and initiation processes transmitting the threshold power (about 1.3 W)

at  $1.48 \mu\text{m}$  [48], [49] and near the stop point in the fast detonation-like mode of fiber fuse propagation under kW-range laser radiation [17].



**Figure 8.** Relationship between  $l/\Lambda$  and the nonlinearity parameter  $\zeta$ .  $\epsilon = 7.5$ ,  $\beta = 6.5$ .

Furthermore, the rapid changes of  $l/\Lambda$  values (or irregular cavity tracks) were observed near the splicing point of HI 1060 and SMF-28e fibers [50]. Todoroki reported that irregular cavity tracks remained over hetero-core splice points of HI 1060 and SMF-28e fiber pairs when an Yb fiber laser at  $\lambda_0 = 1.07 \mu\text{m}$  and  $P_0 = 9 \text{ W}$  was injected to the end of an HI 1060 fiber [50]. Since the pump light propagates in the multimode in SMF-28e, its energy density is lower than that in HI 1060. Thus, the occurrence of an irregular cavity track seems to be caused by the light intensity modulation of hetero-core splicing. That is, a stable propagation mode in the HI 1060 or SMF-28e fiber becomes an unstable transient mode at the hetero-core splicing point, and returns to the stable propagation mode in the SMF-28e or HI 1060 fiber after passing through the splicing point.

From these observations it may be concluded that thermodynamic instability owing to the rapid temperature increase and/or decrease, the light intensity modulation, and so forth results in the increase or decrease in the  $l/\Lambda$  of the cavity, which tends to be 0.5 under a thermodynamically stable condition.

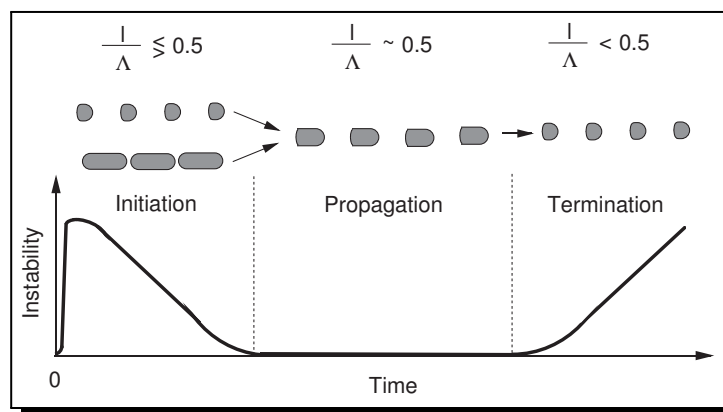


**Figure 9.** Cavity patterns observed in fiber fuse initiation, propagation, and termination processes.

Figure 9 shows a schematic view of the  $l/\Lambda$  values in the fiber fuse initiation, propagation, and termination processes. In the initiation process, thermodynamic instability is very high owing to rapid increase in temperature of the core, melting and vaporization of the core material. In the initiation process,  $l/\Lambda$  takes the value of  $<$  or  $>$  0.5. Then the instability decreases and approaches to zero after the passage of time and the next process (fiber fuse propagation) begins. In fiber fuse propagation,  $l/\Lambda$  maintains the value of about 0.5. And when the termination process occurs, thermodynamic instability increases with increasing of time, and  $l/\Lambda$  decreases to be the value of  $<$  0.5.

#### 4. Population Dynamics of Interacting Self-Oscillators in Ionized Gas Plasma

The Van der Pol oscillator is a classical model for self-oscillating relaxation systems which, after initial amplitude growth, reach a limit cycle in phase space due to a nonlinear saturation mechanism [26], [56].

It was found that the fiber fuse initiation process at which the cavities are formed consists of two steps: the generation of a precursor in a hot spot and the transition to a steady state of fiber fuse propagation out of the hot spot [47]. It can be assumed that a large population of coupled limit-cycle oscillators is a useful model in studies of self-synchronization phenomena observed in the initiation process of the fiber fuse.

In the first step, the oscillators in the hot spot are considered to be similar to each other, although they cannot be strictly identical. Specifically, their natural frequencies may be distributed over a certain range. Even if the frequencies are essentially identical in nature, they cannot be perfectly free from environmental fluctuations. In any case, such randomness factors are destructive to mutual entrainment or to the formation of coherent rhythmicity. In contrast, coupling among the oscillators usually favors mutual synchronization. The conflict between such opposing tendencies is common to all types of phase transitions [5].

If the coupling strength becomes sufficiently large to compensate the desynchronizing effect due to the dispersion of natural frequencies, a macroscopic cluster of mutually entrained oscillators with a common frequency appears, and thus global oscillations of the population occur, that is, a fiber fuse is generated.

To investigate such a phenomenon, phase models are most frequently used. An attempt to describe populations of oscillators in terms of phases was made by Winfree [57]. There have been some attempts to make his idea more precise in some respects [2], [22], [9–11], [31–33], [37–40], [44]. Kuramoto and coworkers and Daido developed a phase description method using simple forms, which are derived by averaging underlying equations when the dispersion of natural frequencies as well as the coupling is weak [9–11], [31–33], [37–40]. Among them, the following class of models with uniform coupling appears to be particularly simple:

$$\frac{d\phi_j}{dt} = \omega_j - \frac{K}{N} \sum_{k=1}^N \sin(\phi_j - \phi_k), \quad (j = 1, 2, \dots, N) \quad (4.1)$$

where  $N$  is the number of oscillators,  $\phi_j$  and  $\omega_j$  are the phases and natural frequencies of the constituent oscillators, respectively, and  $K$  is the coupling strength of the interacting oscillators.

The natural frequencies  $\omega_j$  are constant in time and are distributed randomly. This model shown in Eq. (4.1) is called the Kuramoto model [2], [44]. The normalized number density of oscillators having natural frequencies  $\omega$  is denoted as  $g(\omega)$ . To simplify the analysis we treat the case that  $g(\omega)$  is symmetric about the mean value  $\omega_0$ .

In analogy to thermodynamic phase transitions, it is appropriate to define an order parameter. A convenient choice for this is the complex quantity  $\sigma \exp(i\theta)$  defined by

$$\sigma \exp(i\theta) = \frac{1}{N} \sum_{k=1}^N \exp(i\phi_j), \quad (4.2)$$

where  $\theta = \omega_0 t$  [37]. Equation (4.1) is rewritten using Eq. (4.2) as

$$\frac{d\phi_j}{dt} = \omega_j - K\sigma \sin(\phi_j - \theta), \quad (4.3)$$

which shows that each oscillator is subject to an internal field whose strength is  $K\sigma$ .

The fraction  $r$  of the population forming a synchronized cluster can be calculated as follows:

$$r = \frac{N_s}{N} = \int_{\omega_0 - K\sigma}^{\omega_0 + K\sigma} g(\omega) d\omega \approx 2K\sigma g(\omega_0), \quad (4.4)$$

where  $N_s$  is the number of oscillators forming the synchronized cluster.

On the other hand, the distribution of the effective frequencies  $\tilde{\omega}$ , which is related to that of the natural frequencies  $\omega$ , is denoted as  $G(\tilde{\omega})$ .  $G$  can be conveniently expressed as a sum of synchronized and desynchronized parts [33]:

$$G(\tilde{\omega}) = G_s(\tilde{\omega}) + G_{ds}(\tilde{\omega}). \quad (4.5)$$

The synchronized part is concentrated around frequency  $\omega_0$ , i.e.,

$$G_s(\tilde{\omega}) = r\delta(\tilde{\omega} - \omega_0). \quad (4.6)$$

The desynchronized part is given by [33]

$$G_{ds}(\tilde{\omega}) = g\left(\omega_0 + \sqrt{(\tilde{\omega} - \omega_0)^2 + (K\sigma)^2}\right) \frac{|\tilde{\omega} - \omega_0|}{\sqrt{(\tilde{\omega} - \omega_0)^2 + (K\sigma)^2}}. \quad (4.7)$$

We consider the simple case of  $g$  being symmetric about its maximum at  $\omega_0$ . If  $g(\omega)$  is a Lorentzian,

$$g(\omega) = \frac{\gamma}{\pi} \frac{1}{(\omega - \omega_0)^2 + \gamma^2}, \quad (4.8)$$

where  $\gamma$  is the half width at half maximum,  $\sigma$  is given by [32], [33]

$$\sigma = \begin{cases} \sqrt{1 - 2\gamma/K}, & 2\gamma \leq K, \\ 0, & 2\gamma > K. \end{cases} \quad (4.9)$$

The distribution  $G(\tilde{\omega})$  is given by [31]–[33]

$$G(\tilde{\omega}) = r\delta(\tilde{\omega} - \omega_0) + \frac{\gamma}{\pi} \frac{|\tilde{\omega} - \omega_0|}{[(\tilde{\omega} - \omega_0)^2 + (K\sigma)^2 + \gamma^2] \sqrt{(\tilde{\omega} - \omega_0)^2 + (K\sigma)^2}}. \quad (4.10)$$

$G(\tilde{\omega}) (= G_s(\tilde{\omega}) + G_{ds}(\tilde{\omega}))$  is shown in Figure 10 in the case of  $2\gamma/K = 0.5$  together with  $g(\omega)$ . In this figure,  $\gamma = 1$  and  $\omega_0 = 0$  are assumed.

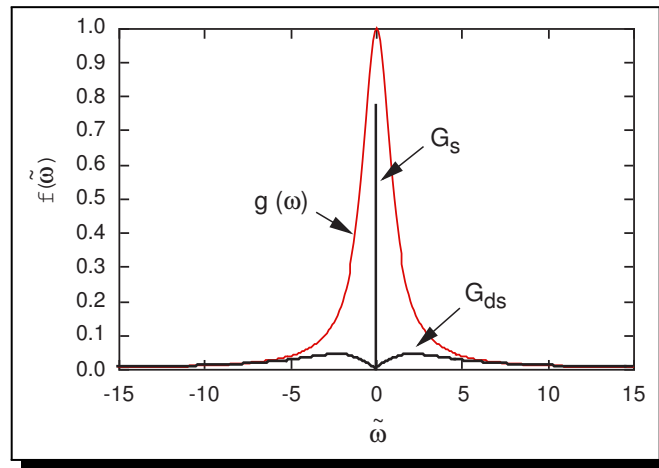


**Figure 10.** Distribution of the effective frequencies  $\tilde{\omega}$  when  $2\gamma/K = 0.5$ ,  $\gamma = 1$ ,  $\omega_0 = 0$ .

As shown in Figure 10, a sharp population drop in  $G_{ds}$  occurs near the frequency of synchronization ( $\omega_0$ ). This seems to reflect the fact that the frequencies of the oscillators whose natural frequencies are close to  $\omega_0$  are shifted perfectly to the central frequency to form a sharp peak, resulting in a rapid population decrease around this peak.

Using  $K$  and  $\gamma$ , the parameter  $r$  is given by [31–33]

$$r = \begin{cases} (2/\pi)\tan^{-1}(K\sqrt{1-2\gamma/K}/\gamma), & 2\gamma \leq K, \\ 0, & 2\gamma > K. \end{cases} \tag{4.11}$$

The relationship between  $r$  and  $K/\gamma$  is illustrated in Figure 11.

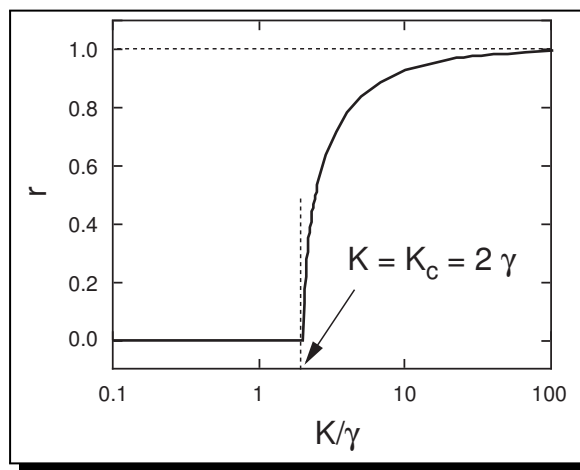


**Figure 11.** Relationship between  $r$  and  $K/\gamma$ .

As shown in Figure 11, when the coupling strength  $K$  becomes larger than  $2\gamma$ , a macroscopic cluster of mutually entrained oscillators with a common frequency  $\omega_0$  gradually appears, and finally coherent rhythmicity (that is, the formation of a fiber fuse) is achieved when  $K \sim 10\gamma$ .

## 5. Relationship between Mutual Entrainment and Periodic Cavity Interval

Todoroki reported the  $P_0$  dependence of  $\Lambda$  in an SMF-28e fiber at  $\lambda_0 = 1.48 \mu\text{m}$  [48], [52]. In this study, we investigated the  $P_0$  dependence of  $\Lambda$  on the basis of the population dynamics of interacting self-oscillators.

The oscillatory motion for  $\epsilon = 7.5$ ,  $\beta = 6.5$ , and  $\zeta = 0$  was calculated using Eq. (2.1) in the two cases of  $r \sim 0$  and  $r \sim 1$ . The calculated results are shown in Figures 12 and 13, respectively, where the perturbed density  $\rho_1$  is plotted as a function of time and  $\Phi$  is the period between the peaks of the  $\rho_1$  values.

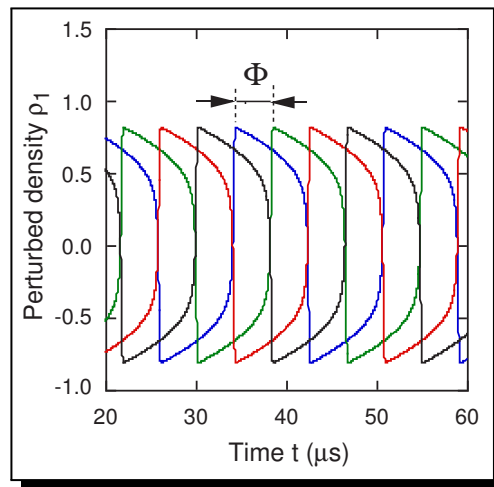


**Figure 12.** Time dependence of the perturbed density when  $r \sim 0$  and  $N = 4$ .  $\epsilon = 7.5$ ,  $\beta = 6.5$ ,  $\zeta = 0$ .

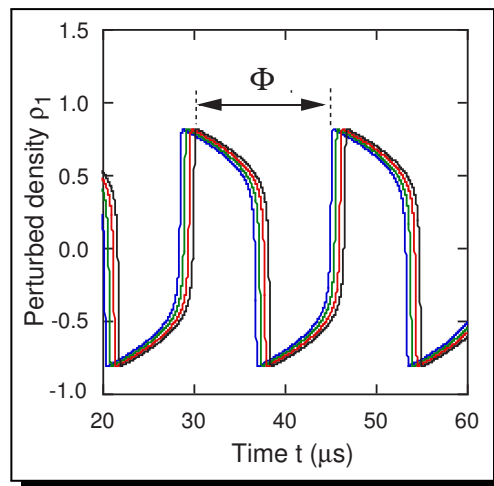


**Figure 13.** Time dependence of the perturbed density when  $r \sim 1$  and  $N = 4$ .  $\epsilon = 7.5$ ,  $\beta = 6.5$ ,  $\zeta = 0$ .

In Figure 12,  $\Phi$  approaches 0 as  $N \rightarrow \infty$ . As shown in Figures 12 and 13,  $\Phi$  in the case of  $r \sim 0$  is smaller than that in the case of  $r \sim 1$ .

The relationship between the period  $\Phi$  and the cavity interval  $\Lambda$  is given by Eq. (2.3). If the same  $V_f$  value is assumed in the cases of  $r \sim 0$  (Figure 12) and  $r \sim 1$  (Figure 13), the increase in  $r$  results in the increase in  $\Lambda$ .

This  $r$  is the fraction of the population forming a synchronized cluster among the weakly coupled oscillators. As shown in Figure 11, when the coupling strength  $K$  becomes larger than the threshold value ( $K_C = 2\gamma$ ), a macroscopic cluster of mutually entrained oscillators with a common frequency  $\omega_0$  gradually appears. Similarly, cavities with a periodic interval  $\Lambda$  owing to fiber fuse propagation appear when the input laser power  $P_0$  exceeds the threshold power  $P_{th}$  ( $= 1.3 \text{ W}$  [53]). Therefore, we assume the following relationships between the parameters of the population dynamics and the fiber fuse propagation:

$$\begin{aligned} K &\longleftrightarrow P_0, \\ K_C (= 2\gamma) &\longleftrightarrow P_{th}, \\ r &\longleftrightarrow \Lambda. \end{aligned}$$

The following relationships between them are also assumed:

$$\frac{K}{2\gamma} = \frac{P_0}{P_{th}}, \tag{5.1}$$

$$r = \frac{\Lambda}{C}, \tag{5.2}$$

where  $C$  is a constant. By substituting Eqs. (5.1) and (5.2) into Eq. (4.11), the following equation is derived for  $\Lambda$ :

$$\Lambda = Cr = \left(\frac{2C}{\pi}\right) \tan^{-1} \left(\frac{2\sqrt{(P_0 - P_{th})P_0}}{P_{th}}\right). \tag{5.3}$$

The relationship between  $\Lambda$  and  $P_0$  was investigated using Eq. (5.3), where  $C = 18.5 \mu\text{m}$  was adopted in the calculation. The calculated results are shown in Figure 14. In this figure, the open circles are the data reported by Todoroki [48], [51].

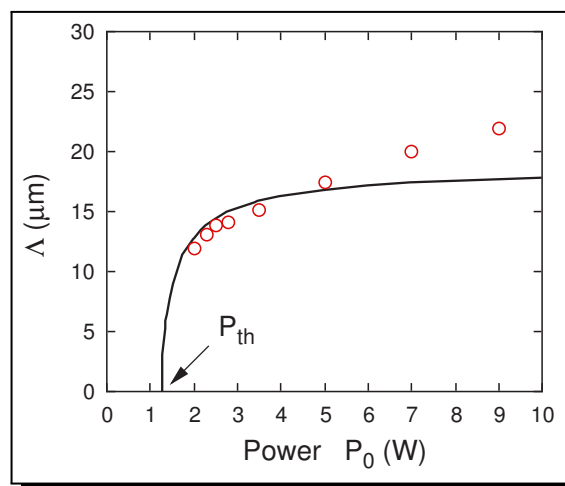


**Figure 14.** Relationship between the interval  $\Lambda$  and the input power  $P_0$ . The solid line was calculated using Eq. (5.3). The open circles are the data reported by Todoroki [48], [51].

As shown in Figure 14,  $\Lambda$  increases abruptly near the threshold power ( $P_{th}$ ) and increases with increasing  $P_0$ . The  $\Lambda$  values at  $P_0 = 2\text{--}5$  W satisfy Eq. (5.3). However, with increasing  $P_0$ , the  $\Lambda$  values at  $P_0 > 5$  W become larger than those calculated using Eq. (5.3).

Todoroki reported that the minimum laser power for fiber fuse initiation was 5.5 W for a conventional optical fiber (SMF-28e+) at  $\lambda_0 = 1.48 \mu\text{m}$  in trials using a fusion splicer when the arc discharge intensity was the same as that for normal fiber splicing. He also found that all the trials with pumping at more than 6 W resulted in the initiation of fiber fuse propagation [47]. It can be considered from these experimental results that the rapid increase in  $\Lambda$  at  $P_{th} \leq P_0 \leq 5$  W shown in Figure 14 corresponds to the first step of the fiber fuse initiation process.

This may be related to the modes of fiber fuse propagation reported by Todoroki [48], [51]. Todoroki classified the damage to the front part of a fiber fuse into three shapes (two spheroids and a long partially cylindrical cavity) depending on the pump power, and the appearance of the long partially cylindrical cavity, which is a typical shape of the cavity, was observed at  $P_0 > 3.5$  W [48] or  $P_0 > 2.3$  W [51]. As shown in Figure 14,  $\Lambda$  tends to be proportional to  $P_0$  at  $P_0 > 3.5$  W. A similar proportional relationship between  $\Lambda$  and  $P_0$  was reported by Atkins *et al.* [4] and Sun *et al.* [45]. This behavior means that the cavity formation process changes from the precursor generation process at  $P_0 < 3.5$  W to the fiber fuse propagation process with long partially cylindrical cavities at  $P_0 > 3.5$  W.

In what follows, we attempt to clarify the relationship between  $\Lambda$  and  $P_0$  in the stable initiation process of fiber fuse propagation at  $P_0 > 6$  W. It is well known that the fiber-fuse propagation velocity  $V_f$ , which is related to  $\Lambda$  as shown on Eq. (2.3), increases with increasing input laser power  $P_0$  [4], [7], [8], [13], [16–18], [23], [24], [29], [43], [45], [48], [51]. In particular,  $V_f$  tends to be proportional to  $P_0$  at  $P_0 > 3.5$  W [48]. As shown in Eq. (2.3), the parameter  $\Lambda/V_f$  equals to the period  $\Phi$ . The experimentally determined  $\Lambda/V_f$  at  $P_0$  of 2–9 W was estimated using the data reported by Todoroki [48], [51] and the  $\Lambda/V_f$  at  $P_0$  of 22 W (7.9 W at  $1.48 \mu\text{m}$  and 14.1 W at  $1.55 \mu\text{m}$ ) was estimated using the data reported by Tsujikawa *et al.* [54]. The calculated results are shown in Figure 15.

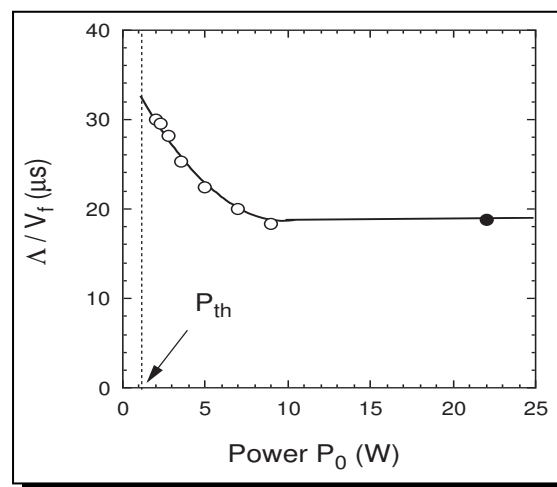


**Figure 15.** Relationship between the parameter  $\Lambda/V_f$  and the input power  $P_0$ . The open circles are the data reported by Todoroki [48], [51] and the closed circle is the data reported by Tsujikawa *et al.* [54].

As shown in Figure 15,  $\Lambda/V_f$  (or  $\Phi$ ) decreases with increasing  $P_0$  and gradually approaches to a constant value of about  $19 \mu\text{s}$  at  $P_0 > 6 \text{ W}$ .

As described above, thermodynamic instability exists in the initiation process at  $P_0 \approx P_{th}$  and this instability disappears when fiber fuse propagation begins. Thus, the decrease in  $\Phi$  (or  $\Lambda/V_f$ ) in the initiation process at  $P_0 < 6 \text{ W}$  is considered to correspond to the decrease in the thermodynamic instability. This instability will gradually decrease with increasing  $P_0$  and disappear at  $P_0 = 6 \text{ W}$ , at which fiber fuse propagation starts. This means that the constant  $\Phi$  (or  $\Lambda/V_f$ ) of about  $19 \mu\text{s}$  is the  $\Phi$  of the thermodynamically stable condition of fiber fuse propagation. As shown in Figure 5, the period  $\Phi$ , which is equal to the  $\Lambda/V_f$ , increases with increasing nonlinearity parameter  $\epsilon$ . The constant  $\Phi$  values of  $19 \mu\text{s}$  correspond to  $\epsilon \sim 8$  as shown in Figure 5.

In closing, we summarize the relationship between the population dynamics (synchronization and desynchronization) of interacting oscillators and the fiber fuse initiation, propagation, and termination processes. Figure 16 shows a schematic view of the relationship between the population dynamics of interacting oscillators and the fiber fuse processes. In the initiation process, where thermodynamic instability is very high, a macroscopic cluster of mutually entrained oscillators with a common frequency  $\omega_0$  gradually appears and the system spontaneously synchronizes. In the propagation process, coherent rhythmicity is achieved and the coherent state is stable. And when the termination process occurs owing to lowering the  $P_0$ , thermodynamic instability increases with increasing of time. In this process, desynchronization of the mutually entrained oscillators occurs and the coherent state becomes unstable.

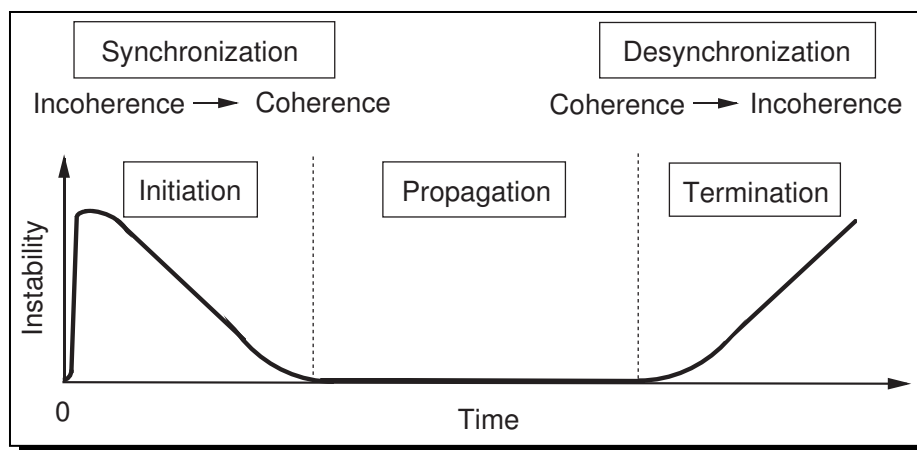


**Figure 16.** Schematic view of the relationship between the population dynamics of interacting oscillators and the fiber fuse initiation, propagation, and termination processes.

## 6. Conclusion

The cavity pattern formation and its dynamics of a fiber fuse in a single-mode optical fiber were studied theoretically. To clarify cavity pattern formation we investigated a nonlinear oscillation model using the Van der Pol equation. This model was able to phenomenologically explain the formation of periodic cavities, the cavity shape, and the regularity of the cavity pattern in the core layer as a result of the relaxation oscillation and cavity compression and/or deformation.

To clarify the power dependence of the periodic cavity interval, we investigated the population dynamics of interacting self-oscillators using the Kuramoto model. When the coupling strength became larger than the threshold value, this model was able to explain the appearance of a macroscopic cluster of mutually entrained oscillators with a common frequency. Similarly, cavities with a periodic interval due to fiber fuse propagation appear when the input laser power  $P_0$  exceeds the threshold power  $P_{th}$ . Therefore, we assumed the relationships between the parameters of the population dynamics and the fiber fuse propagation, and found an equation describing the power dependence of the periodic cavity interval. The experimentally determined cavity intervals at  $P_{th} \leq P_0 \leq 5$  W, corresponding to the precursor generation process of a fiber fuse, satisfied this equation. Furthermore, the experimental cavity intervals in the steady state of fiber fuse propagation at  $P_0 > 6$  W can be explained by considering the power dependence of the propagation velocity of the fiber fuse and the constant period of the Van der Pol oscillator.

### Competing Interests

The author declares that he has no competing interests.

### Authors' Contributions

The author wrote, read and approved the final manuscript.

## References

- [1] K. S. Abedin and M. Nakazawa, Real time monitoring of a fiber fuse using an optical time-domain reflectometer, *Optics Express* **18**(20) (2010), 21315 – 21321, DOI: 10.1364/oe.18.021315.
- [2] J. A. Acebron, L. L. Bonilla, C. J. P. Vicente, F. Ritort and R. Spigler, The Kuramoto model: a simple paradigm for synchronization phenomena, *Reviews of Modern Physics* **77**(1) (2005), 137 – 185, DOI: 10.1103/RevModPhys.77.137.
- [3] P. F. C. Antunes, M. F. F. Domingues, N. J. Alberto and P. S. André, Optical fiber microcavity strain sensors produced by the catastrophic fuse effect, *IEEE Photonics Technology Letters* **26**(1) (2014), 78 – 81, DOI: 10.1109/LPT.2013.2288930.
- [4] R. M. Atkins, P. G. Simpkins and A. D. Yablon, Track of a fiber fuse: a Rayleigh instability in optical waveguides, *Optics Letters* **28**(12) (2003), 974 – 976, DOI: 10.1364/OL.28.000974.
- [5] R. Brout, *Phase Transitions*, Chapter 2, W. A. Benjamin, Inc., New York (1965).
- [6] I. A. Bufetov, A. A. Frolov, E. M. Dianov, V. E. Fortov and V. P. Efremov, Dynamics of fiber fuse propagation, *Optical Fiber Communication Conference and Exposition and The National Fiber Optic Engineers Conference (OFC/NFOEC 2005)*, Optical Society of America, paper OThQ7 (2005), <https://www.osapublishing.org/abstract.cfm?uri=OFC-2005-OThQ7>.
- [7] I. A. Bufetov, A. A. Frolov, V. P. Efremov, M. Y. Schelev, V. I. Lozovoi, V. E. Fortov and E. M. Dianov, Fast optical discharge propagation through optical fibres under kW-range laser radiation, in *Proceedings of 31st European Conference on Optical Communications (ECOC 2005)*, Vol. **6**, pp. 39–40 (2005), DOI: 10.1049/cp:20050866.
- [8] E. D. Bumarín and S. I. Yakovlenko, Temperature distribution in the bright spot of the optical discharge in an optical fiber, *Laser Physics* **16**(8) (2006), 1235 – 1241, DOI: 10.1134/S1054660X06080123.
- [9] H. Daido, Discrete-time population dynamics of interacting self-oscillators, *Progress of Theoretical Physics* **75**(6) (1986), 1460 – 1463, DOI: 10.1143/PTP.75.1460.

- [10] H. Daido, Population dynamics of randomly interacting self-oscillators. I, *Progress of Theoretical Physics* **77**(3) (1987), 622 – 634, DOI: 10.1143/PTP.77.622.
- [11] H. Daido, Order function and macroscopic mutual entrainment in uniformly coupled limit-cycle oscillators, *Progress of Theoretical Physics* **88**(6) (1992), 1213 – 1218, DOI: 10.1143/ptp/88.6.1213.
- [12] D. D. Davis, S. C. Mettler and D. J. DiGiovanni, Experimental data on the fiber fuse, in *Proceedings of 27th Annual Boulder Damage Symposium: Laser-Induced Damage in Optical Materials*, Vol. **2714** (1995), 202 – 210, DOI: 10.1117/12.240382.
- [13] D. D. Davis, S. C. Mettler and D. J. DiGiovanni, A comparative evaluation of fiber fuse models, in *Proceedings of Conference 'Laser-Induced Damage in Optical Materials'*, Vol. **2966** (1996), 592 – 606, DOI: 10.1117/12.274220.
- [14] E. M. Dianov, V. M. Mashinsky, V. A. Myzina, Y. S. Sidorin, A. M. Streltsov and A. V. Chickolini, Change of refractive index profile in the process of laser-induced fibre damage, *Soviet Lightwave Communications* **2** (1992), 293 – 299.
- [15] E. M. Dianov, I. A. Bufetov and A. A. Frolov, Destruction of silica fiber cladding by the fuse effect, *Optics Letters* **29**(16) (2004), 1852 – 1854, DOI: 10.1364/OL.29.001852.
- [16] E. M. Dianov, V. E. Fortov, I. A. Bufetov, V. P. Efremov, A. E. Rakitin, M. A. Melkumov, M. I. Kulish and A. A. Frolov, High-speed photography, spectra, and temperature of optical discharge in silica-based fibers, *IEEE Photonics Technology Letters* **18**(6) (2006), 752 – 754, DOI: 10.1109/LPT.2006.871110.
- [17] E. M. Dianov, V. E. Fortov, I. A. Bufetov, V. P. Efremov, A. A. Frolov, M. Ya. Schelev and V. I. Lozovoi, Detonation-like mode of the destruction of optical fibers under intense laser radiation, *JETP Letters* **83**(2) (2006), 75 – 78, DOI: 10.1134/S002136400602007X.
- [18] F. Domingues, A. R. Frias, P. Antunes, A. O. P. Sousa, R. A. S. Ferreira and P. S. André, Observation of fuse effect discharge zone nonlinear velocity regime in erbium-doped fibres, *Electronics Letters* **48**(20) (2012), 1295 – 1296, DOI: 10.1049/el.2012.2917.
- [19] F. Domingues, P. Antunes, N. Alberto and P. André, Refractive index sensor based on optical fiber void cavities produced by the catastrophic fuse effect, *Advanced Photonics 2013*, **SM4C.3** (2013), DOI: 10.1364/SENSORS.2013.SM4C.3.
- [20] M. F. F. Domingues, T. B. Paixão, E. F. T. Mesquita, N. Alberto, A. R. Frias, R. A. S. Ferreira, H. Varum, P. F. C. Antunes and P. S. André, Liquid hydrostatic pressure optical sensor based on micro-cavity produced by the catastrophic fuse effect, *IEEE Sensors Journal* **15**(10) (2015), 5654 – 5658, DOI: 10.1109/JSEN.2015.2446534.
- [21] M. F. Domingues, C. A. Rodriguez, J. Martins, N. Alberto, C. Marques, M. Ferreira, P. André and P. Antunes, Cost effective in-line optical fiber fabry perot interferometric pressure sensor, *Advanced Photonics 2017 (IPR, NOMA, Sensors, Networks, SPPCom, PS)*, **JTu4A.15** (2017), DOI: 10.1364/IPRSN.2017.JTu4A.15.
- [22] G. B. Ermentrout, Synchronization in a pool of mutually coupled oscillators with random frequencies, *Journal of Mathematical Biology* **22**(1) (1985), 1 – 9, DOI: 10.1007/BF00276542.
- [23] M. Facão, A. Rocha and P. André, Traveling solution of the fuse effect in optical fibers, *IEEE Journal of Lightwave Technology* **29**(1) (2011), 109 – 114, DOI: 10.1109/JLT.2010.2094602.
- [24] D. P. Hand and P. St. J. Russell, Solitary thermal shock waves and optical damage in optical fibers: the fiber fuse, *Optics Letters* **13**(9) (1988), 767 – 769, DOI: 10.1364/OL.13.000767.
- [25] D. P. Hand and P. St. J. Russell, Soliton-like thermal shock-waves in optical fibers: origin of periodic damage tracks, *Fourteenth European Conference on Optical Communication*, pp. 111 – 114 (1988), <https://ieeexplore.ieee.org/document/93535>.

- [26] C. Hayashi, *Nonlinear Oscillations in Physical Systems*, Chapter 2, McGraw-Hill, Inc., New York (1964), <https://press.princeton.edu/books/hardcover/9780691639222/nonlinear-oscillations-in-physical-systems>.
- [27] S. Jiang, L. Ma, X. Fan, B. Wang and Z. He, Real-time locating and speed measurement of fibre fuse using optical frequency-domain reflectometry, *Scientific Reports* **6** (2016), Article number 25585, DOI: 10.1038/srep25585.
- [28] R. Kashyap and K. J. Blow, Observation of catastrophic self-propelled self-focusing in optical fibres, *Electronic Letters* **24**(1) (1988), 47 – 49, DOI: 10.1049/el:19880032.
- [29] R. Kashyap, Self-propelled self-focusing damage in optical fibres, in *Lasers'87: Proceedings of 10th International Conference on Lasers and Applications*, pp. 859 – 866, STS Press, McLean (1988).
- [30] R. Kashyap, High average power effects in optical fibres and devices, in *Proceedings of 'Reliability of Optical Fiber Components, Devices, Systems, and Networks'*, Vol. **4940**, pp. 108–117 (2003), DOI: 10.1117/12.477395.
- [31] Y. Kuramoto, Self-entrainment of a population of coupled non-linear oscillators, in *International Symposium on Mathematical Problems in Theoretical Physics, Lecture Notes in Physics*, Vol. **39**, pp. 420 – 422, Springer-Verlag, New York (1975), DOI: 10.1007/BFb0013365.
- [32] Y. Kuramoto, Cooperative dynamics of oscillator community, *Progress of Theoretical Physics Supplement* **79** (1984), pp. 223 – 240, DOI: 10.1143/PTPS.79.223.
- [33] Y. Kuramoto, *Chemical Oscillations, Waves, and Turbulence*, Springer-Verlag, Tokyo (1984), DOI: 10.1007/978-3-642-69689-3.
- [34] K. Kurokawa and N. Hanzawa, Fiber fuse propagation and its suppression in hole assisted fibers, *IEICE Transactions on Communications* **E94-B**(2) (2011), 384 – 391, DOI: 10.1587/transcom.E94.B.384.
- [35] G.-R. Lin, M. D. Baiad, M. Gagne, W.-F. Liu and R. Kashyap, Harnessing the fiber fuse for sensing applications, *Optics Express* **22**(8) (2014), 8962–8969, DOI: 10.1364/OE.22.008962.
- [36] A. Rocha, P. Antunes, M. F. Domingues, M. Facão and P. André, Detection of fiber fuse effect using FBG sensors, *IEEE Sensors Journal* **11**(6) (2011), 1390 – 1394, DOI: 10.1109/JSEN.2010.2094183.
- [37] H. Sakaguchi and Y. Kuramoto, A soluble active rotator model showing phase transitions via mutual entrainment, *Progress of Theoretical Physics* **76**(3) (1986), 576 – 581, DOI: 10.1143/PTP.76.576.
- [38] H. Sakaguchi, S. Shinomoto and Y. Kuramoto, Local and global self-entrainments in oscillator lattices, *Progress of Theoretical Physics* **77**(5) (1987), 1005 – 1010, DOI: 10.1143/PTP.77.1005.
- [39] H. Sakaguchi, Cooperative phenomena in coupled oscillator systems under external fields, *Progress of Theoretical Physics* **79**(1) (1988), 39 – 46, DOI: 10.1143/PTP.79.39.
- [40] S. Shinomoto and Y. Kuramoto, Phase transitions in active oscillator systems, *Progress of Theoretical Physics* **75**(5) (1986), 1105 – 1110, DOI: 10.1143/PTP.75.1105.
- [41] Y. Shuto, Cavity formation modeling of fiber fuse in single-mode optical fibers, *Advances OptoElectronics* **2017** (2017), Article ID 5728186, 1 – 11, DOI: 10.1155/2017/5728186.
- [42] Y. Shuto, Cavity generation modeling of fiber fuse in single-mode optical fibers, in P. Steglich and F. De Matteis (eds.) *Fiber Optics – From Fundamentals to Industrial Applications*, Chapter 4, IntechOpen, London (2019), DOI: 10.5772/intechopen.74877.
- [43] Y. Shuto, S. Yanagi, S. Asakawa, M. Kobayashi and R. Nagase, Fiber fuse phenomenon in step-index single-mode optical fibers, *IEEE Journal of Quantum Electronics* **40**(8) (2004), 1113 – 1121, DOI: 10.1109/JQE.2004.831635.

- [44] S. H. Strogatz, From Kuramoto to Crawford: exploring the onset of synchronization in populations of coupled oscillators, *Physica D: Nonlinear Phenomena* **143** (2000), 1 – 20, DOI: 10.1016/S0167-2789(00)00094-4.
- [45] J. Sun, Q. Xiao, D. Li, X. Wang, H. Zhang, M. Gong and P. Yan, Fiber fuse behavior in kW-level continuous-wave double-clad field laser, *Chinese Physics B* **25**(1) (2016), 014204-1–014204-4, DOI: 10.1088/1674-1056/25/1/014204.
- [46] S. Todoroki, Quantitative evaluation of fiber fuse initiation probability in typical single-mode fibers, *Optical Fiber Communication Conference (OFC2015)* (Optical Society of America) **W2A.33** (2015), DOI: 10.1364/OFC.2015.W2A.33.
- [47] S. Todoroki, Quantitative evaluation of fiber fuse initiation with exposure to arc discharge provided by a fusion splicer, *Scientific Reports* **6** (2016), Article number 25366, DOI: 10.1038/srep25366.
- [48] S. Todoroki, Origin of periodic void formation during fiber fuse, *Optics Express* **13**(17) (2005), 6381 – 6389, DOI: 10.1364/OPEX.13.006381.
- [49] S. Todoroki, Transient propagation mode of fiber fuse leaving no voids, *Optics Express* **13**(23) (2005), 9248 – 9256, DOI: 10.1364/OPEX.13.009248.
- [50] S. Todoroki, In situ observation of modulated light emission of fiber fuse synchronized with void train over hetero-core splice point, *PLoS ONE* **3**(9) (2008), e3276, DOI: 10.1371/journal.pone.0003276.
- [51] S. Todoroki, Fiber fuse propagation modes in typical single-mode fibers, *Optical Fiber Communication Conference / National Fiber Optic Engineers Conference 2013 (OFC2013)* (Optical Society of America), **JW2A.11** (2013), DOI: 10.1364/NFOEC.2013.JW2A.11.
- [52] S. Todoroki, *Fiber Fuse: Light-Induced Continuous Breakdown of Silica Glass Optical Fiber*, Chapter 3, NIMS Monographs, Springer, Tokyo (2014), DOI: 10.1007/978-4-431-54577-4.
- [53] S. Todoroki, Threshold power reduction of fiber fuse propagation through a white tight-buffered single-mode optical fiber, *IEICE Electronics Express* **8**(23) (2011), 1978 – 1982, DOI: 10.1587/elex.8.1978.
- [54] K. Tsujikawa, K. Kurokawa, N. Hanzawa, S. Nozoe, T. Matsui and K. Nakajima, Hole-assisted fiber based fiber fuse terminator supporting 22 W input, *Optical Fiber Technology* **42** (2018), 24 – 28, DOI: 10.1016/j.yofte.2018.02.009.
- [55] B. van der Pol, The nonlinear theory of electric oscillations, *Proceedings of the Institute of Radio Engineers* **22**(9) (1934), 1051 – 1086, DOI: 10.1109/JRPROC.1934.226781.
- [56] B. van der Pol, On “relaxation oscillations” I, *The London, Edinburgh, and Dublin Philosophical Magazine and Journal of Science* **2** (1926), 978 – 992, DOI: 10.1080/14786442608564127.
- [57] A. T. Winfree, Biological rhythms and behavior of populations of coupled oscillators, *Journal of Theoretical Biology* **16** (1967), 15 – 42, DOI: 10.1016/0022-5193(67)90051-3.
- [58] S. I. Yakovlenko, Plasma behind the front of a damage wave and the mechanism of laser-induced production of a chain of caverns in an optical fibre, *Quantum Electronics* **34**(8) (2004), 765 – 770, DOI: 10.1070/QE2004v034n08ABEH002845.
- [59] S. I. Yakovlenko, Mechanism for the void formation in the bright spot of a fiber fuse, *Laser Physics* **16**(3) (2006), 474 – 476, DOI: 10.1134/S1054660X0603008X.
- [60] S. I. Yakovlenko, Physical processes upon optical discharge propagation in optical fiber, *Laser Physics* **16**(9) (2006), 1273 – 1290, DOI: 10.1134/S1054660X06090015.